First Measurement of Differential Cross Sections for Muon Neutrino Charged Current Interactions on Argon with a Two-proton Final State in the MicroBooNE Detector

P. Abratenko,[34] D. Andrade Aldana,[14] J. Anthony,[4] L. Arellano,[19] J. Asaadi,[33] A. Ashkenazi,[31] S. Balasubramanian,[11] B. Baller,[11] G. Barr,[24] J. Barrow,[20,31] V. Basque,[11] L. Bathe-Peters,[13] O. Benevides Rodrigues,[30] S. Berkman,[11] A. Bhanderi,[19] M. Bhattacharya,[11] M. Bishai,[2] A. Blake,[16] B. Bogart,[21] T. Bolton,[15] J. Y. Book,[13] L. Camilleri,[9] D. Caratelli,[3] I. Caro Terrazas,[8] F. Cavanna,[11] G. Cerati,[11] Y. Chen,[27] J. M. Conrad,[20] M. Convery,[27] L. Cooper-Troendle,[37] J. I. Crespo-Anadón,[5] M. Del Tutto,[11] S. R. Dennis,[4] P. Detje,[4] A. Devitt,[16] R. Diurba,[1,22] R. Dorrill,[14] K. Duffy,[24] S. Dytman,[25] B. Eberly,[29] A. Ereditato,[1] J. J. Evans,[19] R. Fine,[17] O. G. Finnerud,[19] W. Foreman,[14] B. T. Fleming,[37] N. Foppiani,[13] D. Franco,[37] A. P. Furmanski,[22] D. Garcia-Gamez,[12] S. Gardiner,[11] G. Ge,[9] S. Gollapinni,[32,17] O. Goodwin,[19] E. Gramellini,[11] P. Green,[19] H. Greenlee,[11] W. Gu,[2] R. Guenette,[19] P. Guzowski,[19] L. Hagaman,[37] O. Hen,[20] R. Hicks,[17] C. Hilgenberg,[22] G. A. Horton-Smith,[15] B. Irwin,[22] R. Itay,[27] C. James,[11] X. Ji,[2] L. Jiang,[35] J. H. Jo,[37] R. A. Johnson,[7] Y.-J. Jwa,[9] D. Kalra,[9] N. Kamp,[20] G. Karagiorgi,[9] W. Ketchum,[11] M. Kirby,[11] T. Kobilarcik,[11] I. Kreslo,[1] M. B. Leibovitch,[3] I. Lepetic,[26] J.-Y. Li,[10] K. Li,[37] Y. Li,[2] K. Lin,[26] B. R. Littlejohn,[14] W. C. Louis,[17] X. Luo,[3] K. Manivannan,[30] C. Mariani,[35] D. Marsden,[19] J. Marshall,[36] D. A. Martinez Caicedo,[28] K. Mason,[34] A. Mastbaum,[26] N. McConkey,[19] V. Meddage,[15] K. Miller,[6] J. Mills,[34] A. Mogan,[8] T. Mohayai,[11] M. Mooney,[8] A. F. Moor,[4] C. D. Moore,[11] L. Mora Lepin,[19] J. Mousseau,[21] S. Mulleriababu,[1] D. Naples,[25] A. Navrer-Agasson,[19] N. Nayak,[2] M. Nebot-Guinot,[10] J. Nowak,[16] M. Nunes,[30] N. Oza,[17] O. Palamara,[11] N. Pallat,[22] V. Paolone,[25] A. Papadopoulou,[20] V. Papavassiliou,[23] H. B. Parkinson,[10] S. F. Pate,[23] N. Patel,[16] Z. Pavlovic,[11] E. Piasetzky,[31] I. D. Ponce-Pinto,[37] I. Pophale,[16] S. Prince,[13] X. Qian,[2] J. L. Raaf,[11] V. Radeka,[2] M. Reggiani-Guzzo,[19] L. Ren,[23] L. Rochester,[27] J. Rodriguez Rondon,[28] M. Rosenberg,[34] M. Ross-Lonergan,[17] C. Rudolf von Rohr,[1] G. Scanavini,[37] D. W. Schmitz,[6] A. Schukraft,[11] W. Seligman,[9] M. H. Shaevitz,[9] R. Sharankova,[11] J. Shi,[4] A. Smith,[4] E. L. Snider,[11] M. Soderberg,[30] S. Söldner-Rembold,[19] J. Spitz,[21] M. Stancari,[11] J. St. John,[11] T. Strauss,[11] S. Sword-Fehlberg,[23] A. M. Szelc,[10] W. Tang,[32] N. Taniuchi,[4] K. Terao,[27] C. Thorpe,[16] D. Torbunov,[2] D. Totani,[3] M. Toups,[11] Y.-T. Tsai,[27] J. Tyler,[15] M. A. Uchida,[4] T. Usher,[27] B. Viren,[2] M. Weber,[1] H. Wei,[18] A. J. White,[37] Z. Williams,[33] S. Wolbers,[11] T. Wongjirad,[34] M. Wospakrik,[11] K. Wresilo,[4] N. Wright,[20] W. Wu,[11] E. Yandel,[3] T. Yang,[11] L. E. Yates,[11] H. W. Yu,[2] G. P. Zeller,[11] J. Zennamo,[11] and C. Zhang[2]

(The MicroBooNE Collaboration)*

[1] *Universität Bern, Bern CH-3012, Switzerland*
[2] *Brookhaven National Laboratory (BNL), Upton, NY, 11973, USA*
[3] *University of California, Santa Barbara, CA, 93106, USA*
[4] *University of Cambridge, Cambridge CB3 0HE, United Kingdom*
[5] *Centro de Investigaciones Energéticas, Medioambientales y Tecnológicas (CIEMAT), Madrid E-28040, Spain*
[6] *University of Chicago, Chicago, IL, 60637, USA*
[7] *University of Cincinnati, Cincinnati, OH, 45221, USA*
[8] *Colorado State University, Fort Collins, CO, 80523, USA*
[9] *Columbia University, New York, NY, 10027, USA*
[10] *University of Edinburgh, Edinburgh EH9 3FD, United Kingdom*
[11] *Fermi National Accelerator Laboratory (FNAL), Batavia, IL 60510, USA*
[12] *Universidad de Granada, Granada E-18071, Spain*
[13] *Harvard University, Cambridge, MA 02138, USA*
[14] *Illinois Institute of Technology (IIT), Chicago, IL 60616, USA*
[15] *Kansas State University (KSU), Manhattan, KS, 66506, USA*
[16] *Lancaster University, Lancaster LA1 4YW, United Kingdom*
[17] *Los Alamos National Laboratory (LANL), Los Alamos, NM, 87545, USA*
[18] *Louisiana State University, Baton Rouge, LA, 70803, USA*
[19] *The University of Manchester, Manchester M13 9PL, United Kingdom*
[20] *Massachusetts Institute of Technology (MIT), Cambridge, MA, 02139, USA*
[21] *University of Michigan, Ann Arbor, MI, 48109, USA*
[22] *University of Minnesota, Minneapolis, MN, 55455, USA*
[23] *New Mexico State University (NMSU), Las Cruces, NM, 88003, USA*
[24] *University of Oxford, Oxford OX1 3RH, United Kingdom*
[25] *University of Pittsburgh, Pittsburgh, PA, 15260, USA*
[26] *Rutgers University, Piscataway, NJ, 08854, USA*
[27] *SLAC National Accelerator Laboratory, Menlo Park, CA, 94025, USA*
[28] *South Dakota School of Mines and Technology (SDSMT), Rapid City, SD, 57701, USA*
[29] *University of Southern Maine, Portland, ME, 04104, USA*

[30] Syracuse University, Syracuse, NY, 13244, USA
[31] Tel Aviv University, Tel Aviv, Israel, 69978
[32] University of Tennessee, Knoxville, TN, 37996, USA
[33] University of Texas, Arlington, TX, 76019, USA
[34] Tufts University, Medford, MA, 02155, USA
[35] Center for Neutrino Physics, Virginia Tech, Blacksburg, VA, 24061, USA
[36] University of Warwick, Coventry CV4 7AL, United Kingdom
[37] Wright Laboratory, Department of Physics, Yale University, New Haven, CT, 06520, USA
(Dated: August 7, 2023)

We present the first measurement of differential cross sections for charged-current muon neutrino interactions on argon with one muon, two protons, and no pions in the final state. Such interactions leave the target nucleus in a two-particle two-hole state; these states are of great interest, but currently there is limited information about their production in neutrino-nucleus interactions. Detailed investigations of the production of two-particle two-hole states are vital to support upcoming experiments exploring the nature of the neutrino, and the development of the liquid-argon time-projection-chamber has made possible the isolation of such final states in neutrino scattering. Among the many kinematic quantities we measure, the opening angle between the two protons, the angle between the total proton momentum and the muon, and the total transverse momentum of the final state system are most sensitive to the underlying physics processes as embodied in a variety of models. Realistic initial-state momentum distributions are shown to be important in reproducing the data.

The introduction of the liquid argon time projection chamber (LArTPC) [1–4] has revolutionized the field of accelerator-based neutrino physics, allowing a more detailed observation of ionizing radiation in the final state than was previously possible. This development, in turn, has highlighted the need for advanced modeling of neutrino-nucleus, especially neutrino-argon, interactions and detailed measurements to benchmark those models. Cross-section measurements of a variety of different final state topologies for an array of different nuclei are needed to support the development of neutrino interaction models [5]. These models must address both in-medium nuclear modification of the fundamental neutrino interactions and also final-state interactions (FSI) involving the reaction products as they exit the nucleus [6].

One process that probes both neutrino interactions and nuclear effects is the production of two-particle two-hole (2p2h) states in which two nucleons are removed from the nucleus. These states are primarily produced by neutrino interactions where the momentum transfer is shared between two nucleons via the exchange of a virtual meson, known as a meson exchange current (MEC) [6]. In addition, 2p2h states can also be produced by nuclear effects, such as short-range nucleon-nucleon correlations (SRC) [7, 8] and FSI. In the case of SRCs, the neutrino interacts with a nucleon that is part of a correlated nucleon-nucleon pair. The momentum transfer is relayed to a single nucleon, but, because this nucleon is part of a correlated pair, both nucleons are knocked out of the nucleus. In the case of FSI, it is possible for a single nucleon to knock out a second nucleon as it exits the nucleus thereby leading to a 2p2h final state. Observation of 2p2h states in electron scattering has been used to develop the models [9] of 2p2h production in neutrino scattering and the implementation [10] thereof. Correct modeling of 2p2h interactions is of vital importance to neutrino energy reconstruction and precision measurements of neutrino oscillations, but their production cross section has never been measured directly in neutrino scattering.

A final state topology clearly indicative of the production of a 2p2h state is a charged-current (CC) muon neutrino (ν_μ) interaction that results in one muon, two protons, and no charged or neutral pions (CC1μ2p0π). While there is an existing measurement of CC1μ2p0π events on argon, the analysis was statistically limited, unlike this measurement, and no cross sections were extracted [11]. In detectors with a high threshold for proton reconstruction (see for example [12]) the observation of 2 protons in the final state is limited by the small available phase space with 2 high-momentum protons, and thus this final state cannot be distinguished from other CCQE interactions. In this letter, we present the first differential cross section measurements of CC1μ2p0π topologies on argon using data collected from the Micro Booster Neutrino Experiment (MicroBooNE) [13].

MicroBooNE uses a LArTPC detector located at Fermi National Accelerator Laboratory. The detector sits on axis to the Booster Neutrino Beam (BNB) which has an average energy of $\langle E_\nu \rangle = 0.8$ GeV [14] and is located approximately 470 m from the neutrino production target. The detector consists of two components: (1) a TPC, 10.36 m long in the beam direction, 2.56 m wide in the drift direction, and 2.32 m tall; and (2) an optical system comprised of 32 eight-inch photomultiplier tubes (PMTs). The TPC consists of three wire planes, two induction planes and one collection plane, with the PMTs mounted in an array behind the collection plane. Both components are enclosed in a cylindrical cryostat containing 170 metric tons of liquid argon with approximately

* microboone_info@fnal.gov

85 metric tons within the TPC volume. Electronic signals from the TPC and PMTs are recorded and subdivided into two distinct data samples. The first sample, known as on-beam data (BNB data), is collected coincident to a 1.6 μs BNB neutrino spill. The second sample, known as off-beam data (EXT data), is recorded outside of the BNB spill. The purpose of this second sample is to account for electronic noise and the large cosmic muon background caused by the surface location of the MicroBooNE detector. The BNB data and a portion of the EXT data samples are then filtered based on a required minimum amount of activity measured in the PMTs. This study used data from the three-year period 2016-2018, corresponding to 6.79×10^{20} protons on target.

MicroBooNE utilizes the GENIE neutrino event generator [15] to create two samples of simulated neutrino interactions: (1) Overlay Monte Carlo (Overlay MC) which addresses signal events and beam-related backgrounds; and (2) Dirt Monte Carlo (Dirt MC) which addresses backgrounds from neutrino interactions in the material surrounding the cryostat. The simulated events from both samples are then overlaid onto events from an unbiased EXT sample (which is not filtered based on PMT activity) in order to simulate MicroBooNE's cosmic ray background [16]. Furthermore, MicroBooNE utilizes another sample of simulated events generated using the NuWro neutrino event generator [17] for additional studies.

The physics in both the Overlay MC and Dirt MC samples is given by the GENIE MicroBooNE Tune, a version of the GENIE v3.0.6 G18_10a_02_11a model set in which four parameters are tuned to ν_μ CC0π data from the T2K experiment [18]. The four parameters are: (1) the CC quasi-elastic axial mass [19]; (2) the strength of the random phase approximation (RPA) in the Nieves CCQE cross section calculation [20]; (3) the absolute normalization of the CC2p2h cross section [21]; (4) the shape of the CC2p2h cross section. The shape of the CC2p2h cross section is represented by a parameter that linearly interpolates between two models: the Nieves prediction [21] and the empirical prediction [22].

All of the aforementioned samples are processed by the Pandora reconstruction framework [23] to identify and reconstruct neutrino interactions. From the reconstructed products, a series of selection requirements are applied to identify CC1μ2p0π events. The initial selection looks for events that meet three criteria: (1) the reconstructed neutrino vertex is located within a fiducial volume (FV) defined to be at least 10 cm away from any TPC face; (2) there are exactly three tracks, and no showers as determined by Pandora [24]; (3) the three tracks start within 4 cm of the reconstructed neutrino vertex. Particle identification techniques described in Ref. [25] are then used to identify events with a single muon candidate and two proton candidates.

The final event selection required one muon with momentum in the range $0.1 \leq \mathrm{P}_\mu \leq 1.2\,\mathrm{GeV}/c$, two protons, both with momentum in the range $0.3 \leq \mathrm{P}_p \leq 1.0\,\mathrm{GeV}/c$, no charged pions with momentum above $65\,\mathrm{MeV}/c$, no neutral pions of any momentum, and any number of neutrons. The limits on momentum were chosen due to the reconstruction efficiency, which varied with momentum. To benchmark the performance of the selection, the number of simulated CC1μ2p0π events that pass all selection requirements is compared to the number of events generated using the GENIE MicroBooNE tune; the event selection described above achieves an efficiency of 13.0%. More details of the event selection can be found in Ref. [26].

In addition to studying theoretical predictions of 2p2h processes using the GENIE MicroBooNE Tune and NuWro, we consider predictions from three additional GENIE model sets [19]: GENIE v3.0.6 G18_02a_00_000 (GENIE Empirical), GENIE v3.0.6 G18_10a_02_11a (GENIE Nieves), and GENIE v3.2.0 G21_11b_00_000 (GENIE SuSAv2). All three model sets utilize the same models for CC coherent pion production (CCCOH) [27], CC resonant pion production (CCRES), which is based on the Rein-Sehgal prediction, but uses updated form factors [28] and includes lepton mass effects and additional pion production diagrams [29–31], and CC deep inelastic scattering (CCDIS) [32, 33]. The GENIE Empirical and GENIE Nieves also use the same models to predict the neutral current (NC) quasi-elastic (QE), MEC, COH, RES, and DIS interactions. NC interactions are not implemented in GENIE SuSAv2 at this time [19]. Further, the GENIE Empirical and GENIE Nieves model sets both utilize the hA2018 FSI model [34], while the GENIE SuSAv2 model set utilizes the hN2018 FSI model [35]. Note that the GENIE MicroBooNE Tune is identical to the GENIE Nieves model except for the four tuned parameters mentioned previously.

In addition to the two different FSI models, each model set uses distinct models for quasi-elastic (QE) and MEC neutrino interaction modes. These distinctions in QE, MEC, and FSI models are critical as these components all have an impact on 2p2h processes. The GENIE Empirical model set uses the relativistic Fermi gas (RFG) nuclear model [36], the Llewellyn Smith QE model [37], and an empirically derived prediction for MEC interactions [22]. The GENIE Nieves model set uses the local Fermi gas (LFG) nuclear model [38], which is similar to the RFG model but includes considerations for the nuclear density. The Nieves QE [39] model is similar to the Llewellyn Smith QE model, but includes contributions from long range nucleon-nucleon correlations and Coulombic effects. The Nieves MEC model is derived from first principles [21]. The original SuSAv2 model set utilizes the relativistic mean field (RMF) approximation nuclear model [40, 41], which considers relativistic effects in the calculation of the motion of the nucleons in the nucleus. Relativistic effects are also considered in the calculation of the SuSAv2 QE [42] and SuSAv2 MEC [43] predictions by using scaling functions, derived from relativistic assumptions, to scale the cross sections

at high momentum transfers. Although GENIE lacks the option to use an RMF nuclear model directly, it achieves approximate consistency with the RMF-based results by choosing the nucleon initial momentum from an LFG distribution. On top of that, the default nucleon binding energy used in GENIE for the LFG model is replaced for SuSAv2 with an effective value tuned to most closely duplicate the RMF distribution [10, 44].

Using samples of simulated ν_μ CC interactions from each model set, a study was conducted to determine variables sensitive to physics differences between the model sets. One such variable is the opening angle between the protons in the lab frame, $\gamma_{\vec{P}_L,\vec{P}_R}$, defined as:

$$\cos(\gamma_{\vec{P}_L,\vec{P}_R}) = \frac{\vec{P}_L \cdot \vec{P}_R}{|\vec{P}_L|\,|\vec{P}_R|} \tag{1}$$

where $\vec{P}_L$ is the momentum of the leading proton, the proton with the highest momentum, and $\vec{P}_R$ is the momentum of the recoil proton, the second proton in the event. A second sensitive variable is the opening angle between the muon and total proton momentum vector, $\gamma_{\vec{P}_\mu,\vec{P}_{sum}}$, defined as:

$$\cos(\gamma_{\vec{P}_\mu,\vec{P}_{sum}}) = \frac{\vec{P}_\mu \cdot \vec{P}_{sum}}{|\vec{P}_\mu|\,|\vec{P}_{sum}|} \tag{2}$$

where $\vec{P}_\mu$ is the momentum of the muon and $\vec{P}_{sum}$ is the vector addition of the leading and recoil proton momenta. The opening angle between the protons in the lab frame provides information on the effect of the QE and MEC modeling on the proton momentum, while the opening angle between the muon and total proton momentum vectors provides information on the treatment of the outgoing muon momentum in relation to the 2p2h system.

In addition to these two angles, we also identify the magnitude of the momentum transverse to the neutrino beam direction of the final state system, δP_T [45]. The transverse momentum vector of the CC1μ2p0π system ($\delta\vec{P}_T$) is defined as:

$$\delta\vec{P}_T = \vec{P}_T^{\mu} + \vec{P}_T^{L} + \vec{P}_T^{R} \tag{3}$$

where $\vec{P}_T^{\mu}$, $\vec{P}_T^{L}$, and $\vec{P}_T^{R}$ are the transverse momentum vectors of the muon, leading proton, and recoil proton respectively. The magnitude δP_T is sensitive to nuclear effects, with $\delta P_T \neq 0$ indicative of motion between the nucleons in the initial state.

Distributions of selected events as a function of the cosine of $\gamma_{\vec{P}_L,\vec{P}_R}$ can be found in Fig. 1. The colored bands in each histogram represent events selected from the overlay MC subdivided into different final state topologies [Fig. 1(a)] and different interaction modes based on the GENIE MicroBooNE Tune prediction [Fig. 1(b)]. The error bars on the data points are the data statistical uncertainty while the dashed lines represent the uncertainty on the combination of the Overlay MC, Dirt MC, and EXT data (also known as the prediction). This uncertainty includes both the statistical uncertainty of the prediction and systematic uncertainty, which dominates over the data statistical uncertainty for this measurement. Contributions from flux modeling and protons-on-target (POT) counting [46], cross section modeling [18], re-interaction modeling [47], and detector modeling [48] are considered in the calculation of the systematic uncertainties, which was performed using the multiverse techniques described in Section V of Ref. [18]. Uncertainty on the modeling of dirt events is also considered in the systematic uncertainty [49]. We find that our CC1μ2p0π signal, represented by the pink band in Fig. 1(a), constitutes the majority of events selected from the Overlay MC sample with a purity of 65.4%. We also find that the CCMEC process, represented by the magenta band in Fig. 1(b), has a somewhat different shape compared to our signal. This is expected as MEC is not the only contributor to CC1μ2p0π topologies. The comparison of the data points to the prediction shows reasonable shape agreement as well as normalization agreement at the 1σ level. Similar agreement is seen in other kinematic variables studied in this analysis [26].

Due to detector resolution, efficiency, and smearing effects, our reconstructed kinematic variables require unfolding. We use the D'Agostini iterative Bayesian unfolding procedure [50], as implemented in the RooUnfold software framework [51], for this purpose. We determine the optimal number of iterations using the "L-curve" technique described in Ref. [52] and in section 8.3.1 of Ref. [26]; briefly, this technique optimizes the smoothness of the solution while also minimizing the number of iterations required. We use two unfolding iterations for the distribution of $\cos(\gamma_{\vec{P}_L,\vec{P}_R})$, four unfolding iterations for the distribution of $\cos(\gamma_{\vec{P}_\mu,\vec{P}_{sum}})$, and two unfolding iterations for the distribution of δP_T. The uncertainty associated with the unfolding is determined by comparing the result of a single iteration and that of the total number of iterations (two or four). Unfolded distributions are then normalized by the detector efficiency, number of target nuclei, and the total integrated neutrino flux to produce a cross section.

Fig. 2 shows the single differential cross sections as functions of the cosine of $\gamma_{\vec{P}_L,\vec{P}_R}$ [Fig. 2(a)] and of the cosine of $\gamma_{\vec{P}_\mu,\vec{P}_{sum}}$ [Fig. 2(b)]. The black points represent the extracted cross section from data with the inner error bands representing the statistical uncertainty and the outer error bands representing the systematic uncertainty. The systematic uncertainties include both an overall normalization contribution (9.3%) and also a point-to-point ("shape") contribution (11.4%), while the statistical uncertainty is 4.5%. Although MEC modeling uncertainties enter predominantly only through the

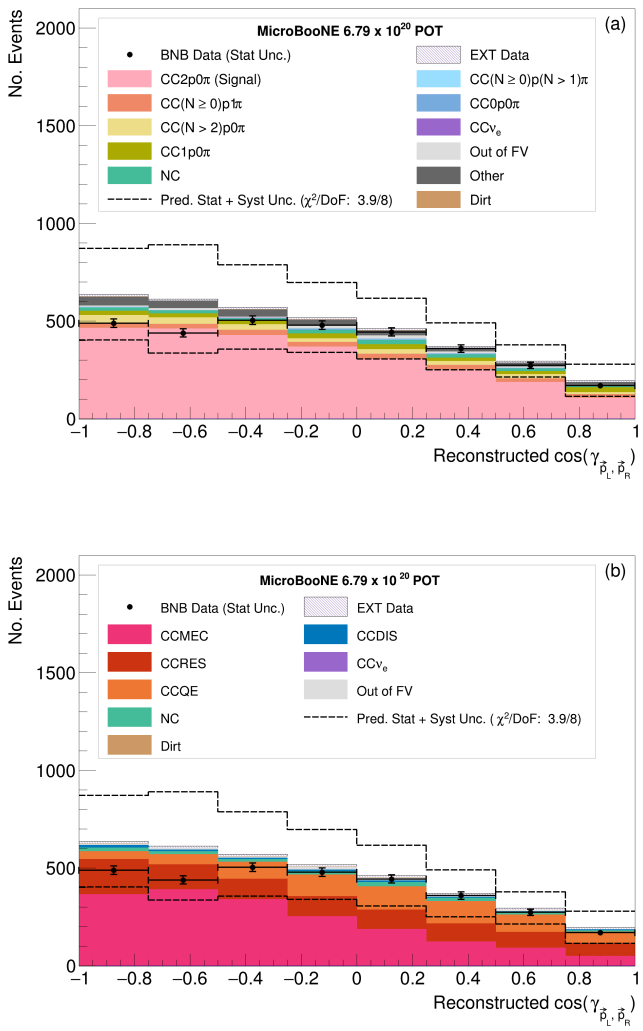

FIG. 1: Yield for the cosine of the opening angle between the protons in the lab frame, $\cos(\gamma_{\vec{P}_L,\vec{P}_R})$. The selected MC events are broken down into (a) final-state topologies and (b) ν interaction channels based on the MicroBooNE Tune [18] truth information. The error on the data represents the data statistical uncertainty and the dashed lines represent the statistical plus systematic uncertainty on the prediction. Note that the Out of FV (grey band) in both plots represents simulated events originating outside of the FV but for which the reconstructed neutrino vertex fell inside of the FV.

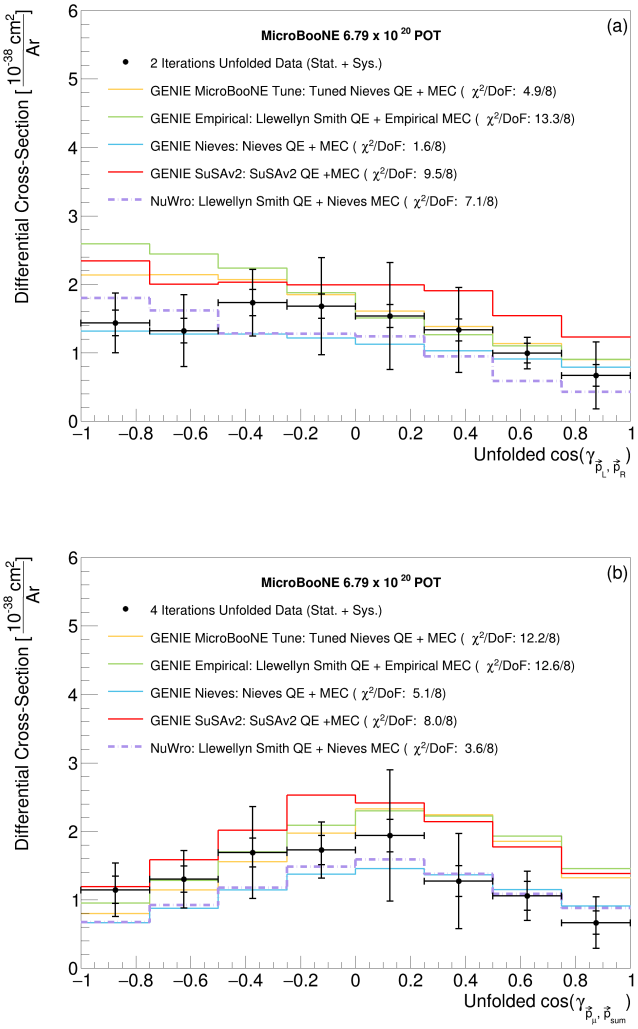

FIG. 2: Single differential cross sections as a function of (a) the cosine of the opening angle between the protons in the lab frame, $\cos(\gamma_{\vec{P}_L,\vec{P}_R})$, and of (b) the cosine of the opening angle between the muon and total proton momentum vector, $\cos(\gamma_{\vec{P}_\mu,\vec{P}_{sum}})$. The inner error bands on the data represent the statistical uncertainty while the outer error bands represent the systematic uncertainty. A χ^2/DoF, considering systematic and statistical uncertainties, is calculated between the data and each model set curve.

efficiency, they are still the dominant cross section uncertainties in some bins due to the large uncertainties assigned to this model which is itself due to the lack of previous measurements. Fake data tests using NuWro were used to verify the analysis. In addition to the six sources of systematic uncertainty mentioned above, an uncertainty on the choice of the number of unfolding iterations is also included in the systematic error band. The cross sections for the GENIE Empirical, GENIE Nieves, and GENIE SuSAv2 model sets were derived using methods described in Ref. [53]. The GENIE MicroBooNE Tune and NuWro cross section curves are created by selecting generated CC1μ2p0π signal events from the Overlay MC and NuWro samples, respectively. Each distribution was then normalized by the number of target nucleons and the total integrated flux to produce a cross section curve. The χ^2 per degree of freedom (χ^2/DoF) is calculated between the data and each model set curve. The

systematic and statistical uncertainties on the data are considered in this calculation using the total covariance matrices found in the Supplemental Materials [54].

We find that the GENIE MicroBooNE Tune and the GENIE Nieves models have the best agreement with our data for $\cos(\gamma_{\vec{P}_L,\vec{P}_R})$, and the GENIE Nieves and NuWro models have the best agreement with our data for $\cos(\gamma_{\vec{P}_\mu,\vec{P}_{sum}})$. We also find that the GENIE Nieves and NuWro models have the best agreement with our data across the full ranges of $\cos(\gamma_{\vec{P}_\mu,\vec{P}_{sum}})$ and $\cos(\gamma_{\vec{P}_\mu,\vec{P}_{sum}})$. The GENIE MicroBooNE Tune and GENIE Empirical models tend to predict higher cross sections than indicated by our data in regions of low $\cos(\gamma_{\vec{P}_L,\vec{P}_R})$ and high $\cos(\gamma_{\vec{P}_\mu,\vec{P}_{sum}})$. Although the GENIE MicroBooNE Tune uses all the same model elements as the GENIE Nieves sample, we find an overall difference in shape and normalization between these two curves. This is most likely caused by the increased CC2p2h cross section normalization and interpolated CC2p2h cross section shape that are utilized in the GENIE MicroBooNE Tune.

We show the single differential cross sections for the data and the models as functions of δP_T in Fig. 3. In this variable the NuWro prediction is higher than the data and other models in the first bin. The reason for this is that Nieves and NuWro form their initial hadronic states in different ways. In the GENIE implementation of the GENIE Nieves model set, two nucleons are selected from the Fermi sea of the nucleus [22]. The momentum of each nucleon is then randomly sampled from a distribution of the initial state nucleon momentum [21] formed from the LFG nuclear model [38]. In NuWro, the selection of the two nucleons and their momenta is similar to the GENIE implementation of GENIE Nieves, but the two nucleons are required to have back-to-back momenta in the initial state [55]. The over-prediction of NuWro at low δP_T has also been observed in Ref. [56], which also finds this over-prediction in the absence of FSI, indicating that the excess is an initial state effect. Our data indicates that there is a preference for the GENIE description of the initial two-nucleon hadronic state. Cross section values for different kinematic variables can be found in the Supplemental Material [54].

In summary, this letter presents the first measurement of single differential cross sections of CC1μ2p0π events on argon. Events containing exactly one muon, two protons, and no other mesons are selected from BNB data. We extract differential cross sections as functions of three kinematic variables, $\cos(\gamma_{\vec{P}_L,\vec{P}_R})$, $\cos(\gamma_{\vec{P}_\mu,\vec{P}_{sum}})$ and δP_T, which are found to be sensitive to the formation of 2p2h pairs through MEC processes. We compare our extracted cross sections to those predicted by the NuWro and GENIE generators, including four different GENIE model sets. These cross-section models span a range of nuclear models, QE and MEC models, and hadron transport models. We find that the NuWro and GENIE Nieves predictions show the best overall shape agreement in the kinematic variables describing opening angles. The δP_T variable is sensitive to the different way that NuWro and GENIE Nieves form the initial hadronic state, and we are therefore able to show that GENIE Nieves gives the best overall description of the production of CC1μ2p0π final states thanks to its more realistic initial-state momentum distributions. None of the models used for comparisons in this work include SRCs in the nuclear model; their inclusion could further improve the agreement with our measured differential cross sections. This is the first direct measurement of the CC2p2h cross section, and therefore the first time that these models can be directly compared to data. This will provide valuable input for future model development toward precision neutrino physics measurements. In addition, these measured CC1μ2p0π cross sections can be used to reinterpret data from existing experiments that cannot distinguish 2p2h final states from other CC interaction mechanisms.

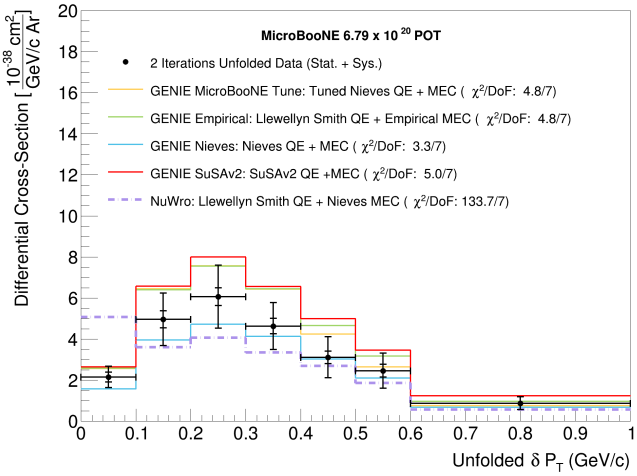

FIG. 3: Single differential cross section as a function of the magnitude of the transverse momentum of the final state system, $\delta P_T = \left|\vec{P}_T^{\mu} + \vec{P}_T^{L} + \vec{P}_T^{R}\right|$. The inner error bands on the data represent the statistical uncertainty while the outer error bands represent the systematic uncertainty. A χ^2/DoF, considering systematic and statistical uncertainties, is calculated between the data and each model set curve.

This document was prepared by the MicroBooNE collaboration using the resources of the Fermi National Accelerator Laboratory (Fermilab), a U.S. Department of Energy, Office of Science, HEP User Facility. Fermilab is managed by Fermi Research Alliance, LLC (FRA), acting under Contract No. DE-AC02-07CH11359. MicroBooNE is supported by the following: the U.S. Department of Energy, Office of Science, Offices of High Energy Physics and Nuclear Physics; the U.S. National Science Foundation; the Swiss National Science Foundation; the

Science and Technology Facilities Council (STFC), part of the United Kingdom Research and Innovation; the Royal Society (United Kingdom); and the UK Research and Innovation (UKRI) Future Leaders Fellowship. Additional support for the laser calibration system and cosmic ray tagger was provided by the Albert Einstein Center for Fundamental Physics, Bern, Switzerland. We also acknowledge the contributions of technical and scientific staff to the design, construction, and operation of the MicroBooNE detector as well as the contributions of past collaborators to the development of MicroBooNE analyses, without whom this work would not have been possible. For the purpose of open access, the authors have applied a Creative Commons Attribution (CC BY) public copyright license to any Author Accepted Manuscript version arising from this submission.

[1] C. Rubbia, Reports No. CERN-EP-INT-77-08 **CERN-EP-77-08** (1977).
[2] H. H. Chen, P. E. Condon, B. C. Barish, and F. J. Sciulli, FNAL Proposal 496 (1976).
[3] W. Willis and V. Radeka, Nucl. Instrum. Methods **120**, 221 (1974).
[4] D. R. Nygren, eConf **C740805**, 58 (1974).
[5] J. A. Formaggio and G. P. Zeller, Rev. Mod. Phys. **84**, 1307 (2012).
[6] L. Alvarez-Ruso and other, Progress in Particle and Nuclear Physics **100**, 1 (2018).
[7] O. Hen, G. A. Miller, E. Piasetzky, and L. B. Weinstein, Rev. Mod. Phys. **89**, 045002 (2017).
[8] R. Cruz-Torres *et al.*, Nature Phys. **17**, 306 (2021), arXiv:1907.03658 [nucl-th].
[9] I. Ruiz Simo, J. Amaro, M. Barbaro, J. Caballero, G. Megias, and T. Donnelly, Annals of Physics **388**, 323 (2018).
[10] S. Dolan, G. D. Megias, and S. Bolognesi, Phys. Rev. D **101**, 033003 (2020).
[11] R. Acciarri *et al.*, Phys. Rev. D **90**, 012008 (2014).
[12] K. Abe *et al.* (The T2K Collaboration), Phys. Rev. D **98**, 032003 (2018).
[13] R. Acciarri *et al.* (MicroBooNE), J. Instrum. **12**, P02017 (2017), arXiv:1612.05824 [physics.ins-det].
[14] A. A. Aguilar-Arevalo *et al.* (MiniBooNE), Phys. Rev. D **79**, 072002 (2009).
[15] C. Andreopoulos *et al.*, Nucl. Instrum. Meth. A **614**, 87 (2010), arXiv:0905.2517 [hep-ph].
[16] C. Adams *et al.* (MicroBooNE), Eur. Phys. J. C **79**, 673 (2019), arXiv:1812.05679 [physics.ins-det].
[17] T. Golan, J. T. Sobczyk, and J. Zmuda, Nucl. Phys. B Proc. Suppl. **229-232**, 499 (2012).
[18] P. Abratenko *et al.* (MicroBooNE), Phys. Rev. D **105**, 072001 (2022), arXiv:2110.14028 [hep-ex].
[19] L. Alvarez-Ruso *et al.* (GENIE), Eur. Phys. J. ST **230**, 4449 (2021), arXiv:2106.09381 [hep-ph].
[20] J. Nieves, J. E. Amaro, and M. Valverde, Phys. Rev. C **70**, 055503 (2004).
[21] J. Schwehr, D. Cherdack, and R. Gran, (2016), arXiv:1601.02038 [hep-ph].
[22] T. Katori, AIP Conf. Proc. **1663**, 030001 (2015), arXiv:1304.6014 [nucl-th].
[23] R. Acciarri *et al.* (MicroBooNE), Eur. Phys. J. C **78**, 82 (2018), arXiv:1708.03135 [hep-ex].
[24] W. Van De Pontseele, Search for Electron Neutrino Anomalies with the MicroBooNE Detector, Ph.D. thesis, Oxford U. (2020).
[25] P. Abratenko *et al.* (MicroBooNE), J. High Energy Phys. **12**, 153 (2021), arXiv:2109.02460 [physics.ins-det].
[26] S. Sword-Fehlberg, First Measurement Of Charged-Current 1 Muon 2 Proton 0 Pion Single Differential Cross-Sections on Argon-40 at 0.8 GeV Average Neutrino Energy with The MicroBooNE Detector, Ph.D. thesis, New Mexico State U. (2022).
[27] C. Berger and L. M. Sehgal, Phys. Rev. D **79**, 053003 (2009), arXiv:0812.2653 [hep-ph].
[28] K. M. Graczyk and J. T. Sobczyk, Phys. Rev. D **77**, 053003 (2008).
[29] C. Berger and L. M. Sehgal, Phys. Rev. D **76**, 113004 (2007).
[30] K. S. Kuzmin, V. V. Lyubushkin, and V. A. Naumov, Mod. Phys. Lett. A **19**, 2815 (2004), arXiv:hep-ph/0312107.
[31] J. A. Nowak (MiniBooNE), AIP Conf. Proc. **1189**, 243 (2009), arXiv:0909.3659 [hep-ph].
[32] U. K. Yang and A. Bodek, Eur. Phys. J. C **13**, 241 (2000), arXiv:hep-ex/9908058.
[33] A. Bodek and U. K. Yang, J. Phys. G **29**, 1899 (2003), arXiv:hep-ex/0210024.
[34] D. Ashery *et al.*, Phys. Rev. C **23**, 2173 (1981).
[35] L. A. Harewood and R. Gran, Unpublished (2019), arXiv:1906.10576 [hep-ex].
[36] R. A. Smith and E. J. Moniz, Nucl. Phys. B **43**, 605 (1972), [Erratum: Nucl.Phys.B 101, 547 (1975)].
[37] C. H. Llewellyn Smith, Phys. Rept. **3**, 261 (1972).
[38] J. Nieves, J. E. Amaro, and M. Valverde, Phys. Rev. C **70**, 055503 (2004).
[39] J. Nieves, F. Sanchez, I. Ruiz Simo, and M. J. Vicente Vacas, Phys. Rev. D **85**, 113008 (2012), arXiv:1204.5404 [hep-ph].
[40] B. D. Serot and J. D. Walecka, "Relativistic nuclear many-body theory," in *Recent Progress in Many-Body Theories: Volume 3*, edited by T. L. Ainsworth *et al.* (Springer US, Boston, MA, 1992) pp. 49–92.
[41] J. A. Caballero, J. E. Amaro, M. B. Barbaro, T. W. Donnelly, C. Maieron, and J. M. Udias, Phys. Rev. Lett. **95**, 252502 (2005).
[42] S. Dolan, G. D. Megias, and S. Bolognesi, Phys. Rev. D **101**, 033003 (2020).
[43] T. W. Donnelly and I. Sick, Phys. Rev. Lett. **82**, 3212 (1999), arXiv:nucl-th/9809063.
[44] A. Papadopoulou *et al.* ($e4\nu$), Phys. Rev. D **103**, 113003 (2021).
[45] S. Dolan (T2K), in *Prospects in Neutrino Physics* (2016) arXiv:1605.00179 [hep-ex].
[46] A. A. Aguilar-Arevalo *et al.* (MiniBooNE), Phys. Rev. D **88**, 032001 (2013), arXiv:1301.7067 [hep-ex].
[47] J. Calcutt, C. Thorpe, K. Mahn, and L. Fields, J. Instrum. **16**, P08042 (2021), arXiv:2105.01744 [physics.data-an].
[48] P. Abratenko *et al.* (MicroBooNE), Eur. Phys. J. C **82**,

454 (2022), arXiv:2111.03556 [hep-ex].
[49] P. Abratenko *et al.* (MicroBooNE), Phys. Rev. D **105**, 112005 (2022), arXiv:2110.13978 [hep-ex].
[50] G. D'Agostini, Nucl. Instrum. Meth. A. **362**, 487 (1995).
[51] G. D'Agostini, Unpublished (2010), 10.48550/arxiv.1010.0632.
[52] Dolan, S. (T2K), "What we measure when we measure σ," NuInt 2018, Gran Sasso Science Institue (GSSI), L'Aquila, Italy.
[53] S. Gardiner, Comput. Phys. Commun. **269**, 108123 (2021), arXiv:2101.11867 [nucl-th].
[54] P. Abratenko *et al.* (MicroBooNE), Supplemental Material at [URL will be inserted by publisher].
[55] K. Niewczas and J. T. Sobczyk, Phys. Rev. C **93**, 035502 (2016), arXiv:1511.02502 [hep-ex].
[56] L. Bathe-Peters, Studies of Single-Transverse Kinematic Variables for Neutrino Interactions on Argon, Master's thesis, Berlin Tech U., Harvard U. (2020).